ChemComm

Accepted Manuscript

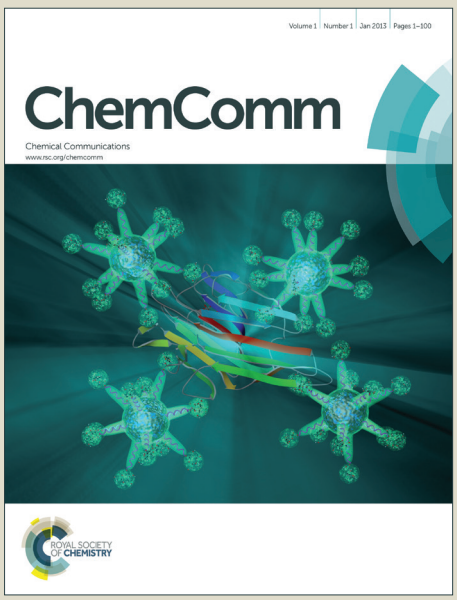

ROYAL SOCIETY OF CHEMISTRY

www.rsc.org/chemcomm

ChemComm

RSCPublishing

COMMUNICATION

Folic acid conjugated silica-titania porous hollow nanosphere for improved topical photodynamic therapy

Cite this: DOI: 10.1039/x0xx00000x

Received 00th January 2014,
Accepted 00th January 2014

DOI: 10.1039/x0xx00000x

www.rsc.org/chemcomm

Yoonsun Jang, Sojin Kim, Wan-Kyu Oh, Chanhoi Kim, Inkyu Lee and Jyongsik Jang*

The folic acid conjugated hollow nanosphere is used to encapsulate protoporphyrin IX and utilized for photodynamic therapy. This system represents 3.33 times higher photodynamic efficiency than previous protoporphyrin IX-based systems. The result proposes a new opportunity for effective photodynamic therapy of folate receptor positive tumor cells.

Photodynamic therapy (PDT) is of great interest as an alternative to conventional chemotherapy for cancer treatment. One of the major component of PDT is a photosensitizer (PS); a light-sensitive dye that is stimulated by a specific wavelength of light and generates singlet oxygen ($^1O_2$) and trigger cell death.[1] Protoporphyrin IX (PpIX), used as the PS in this work, has a relatively low dark toxicity and induces an efficient PDT. Conventional PDT requires expensive laser equipment and leads unexpected cell damage.[2] Laser could lead normal cell damage and the related subject have been studied in many papers.[3] In this research, a light-emitting diode (LED) is employed instead of a laser as the light source for PDT and exhibits fewer side effects.

Due to insolubility of PpIX, delivering PpIX to tumor cell effectively has been investigated to enhance the PDT.[4] We selected porous hollow nanospheres (HNSs) (diameter: *ca.* 50 nm) for the PpIX delivery agent; 50 nm sized HNSs are favored in cellular uptake.[5] An HNS has a large hydrophobic cavity with a porous shell, which can contain more PpIX than mesoporous nanoparticles with the same diameter.[6] In addition, HNSs transmit visible light in the region of 400–800 nm; hence, most of the visible light can penetrate into the shells, excite the PpIX inside the HNSs, and generate $^1O_2$. These $^1O_2$ can diffuse out through the mesoporous shell of an HNS and efficiently destroy tumor cells. In this study, a folic acid (FA)-conjugated HNS was fabricated as a PpIX delivery agent. We investigated the PDT effect by *in vitro* studies of both human breast cancer cell lines, *i.e.*, MCF-7 (folate receptor positive; FR+) and SK-BR-3 (folate receptor negative; FR-). FR is overexpressed on MCF-7 human breast cancer cells and has a high binding affinity with FA, which allows FA to act as a targeting ligand for MCF-7 cells.[7] Several strategies were combined to maximize the PDT effect: 1) FA was used as a targeting ligand for active targeting, 2) *ca.* 50 nm HNSs were synthesized for efficient passive targeting and loading of a large amount of PpIX, 3) HNSs are transparent and do not absorb visible light, and 4) an LED was used as the light source to destroy cancer cells at a specific site, while minimizing undesired normal cell damage.

The synthesis of FA–HNS–PpIX is indicated in Fig. 1a. Previously, Choi *et al.* reported the synthesis of a HNS.[8] The HNSs were made by adding the silica-titania core-shell nanospheres (CSNSs) to aqueous ammonium hydroxide (NH_4OH), which dissolved the silica core and redeposited silica on the surface of the titania shells.[9] The HNSs and PpIX were then mixed in dimethyl sulfoxide (DMSO) and stirred for 24 h to encapsulate the PpIX within the HNSs (HNS–PpIX). After loading the PpIX, the surface of the HNSs was modified with FA (FA–HNS–PpIX). Transmission electron microscopy

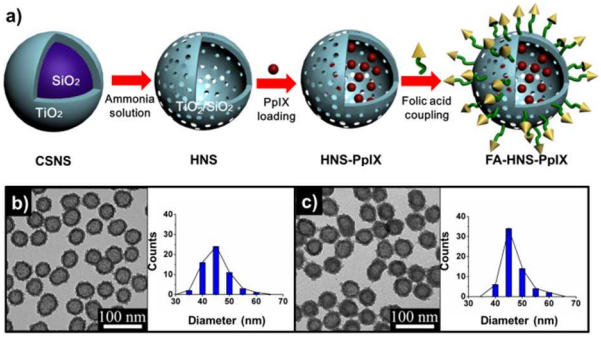

Fig. 1 a) Schematic illustration of the fabrication of FA-HNS-PpIX. TEM images and size distribution histograms of b) HNS and c) FA-HNS.

*World Class University (WCU) program of Chemical Convergence for Energy & Environment (C_2E_2) School of Chemical and Biological Engineering, College of Engineering, Seoul National University (SNU), Seoul, Korea. Fax: 82 2 888 1604; Tel: 82 2 880 7069; E-mail: jsjang@plaza.snu.ac.kr

† *Electronic Supplementary Information (ESI) available: details of synthesis, characterization, and other experimental information. See DOI: 10.1039/c000000x/*

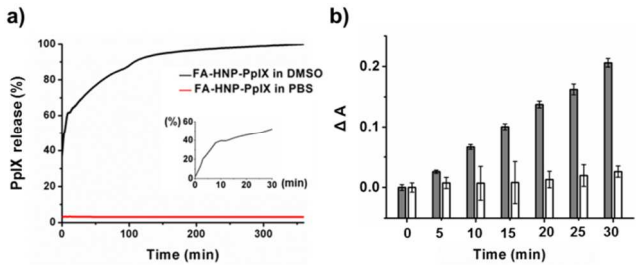

Fig. 2 a) Time dependent cumulative PpIX release profile of FA-HNS-PpIX. Inset: PpIX released from FA-HNS-PpIX in a 30 min. b) The change of absorption intensity of ABDA with and without irradiated FA-HNS-PpIX in different time scale (grey: with irradiation, white: without irradiation).

(TEM) images and size distribution data confirmed that the HNSs had an average diameter of *ca.* 45 nm with a narrow size distribution (Fig. 1b). After FA treatment, the diameter of the HNSs increased by 5 nm, while the dispersity and uniformity in size and shape were still remained (Fig. 1c). The particle size change is caused by the FA conjugation to the surface of the HNS. Moreover, the FT-IR confirmed the synthesis steps (Fig. S1 and Table S1, ESI†). HNS–PpIX had distinguishing peaks at 1076 cm^{-1}, 1724 cm^{-1}, and 2949 cm^{-1}.[10] The characteristic peaks of FA–HNS–PpIX at 698 cm^{-1} and 1261 cm^{-1} demonstrate the successful surface functionalization of FA.[11]

The large hollow cavities and the mesoporous shell of HNSs provide an application as PpIX delivery agent (Fig. S4, ESI†).[5] To investigate this possibility, the loading capacity was evaluated by UV/vis spectroscopy. The loading capacity of the HNSs (484 nM of PpIX are loaded into 1 mg of FA-HNS–PpIX) is about 4.5 times higher loading capacity than that of previous mesoporous nanoparticles.[12] This high loading efficiency demonstrates the great advantages of FA-HNS-PpIX as a hydrophobic photosensitizer loading and suitability for delivery agents. After verifying the aptness of HNSs as a PpIX delivery agent, the solvent dependent release profile of PpIX from FA-HNS-PpIX behavior was studied. In DMSO (hydrophobic PpIX loading environment), PpIX diffused out from the HNSs, while they remained as aggregates inside the HNSs in PBS (hydrophilic biologically similar condition). The FA–HNS–PpIX released about 63.5, 69, and 100% of the PpIX after 15, 30, and 300 min in DMSO (Fig. 2a). However, the FA–HNS–PpIX released very little PpIX in PBS. This result implies that FA-HNS would deliver the PpIX effectively to the inner phase of cancer cells without leakage.

To evaluate the PDT potential of FA-HNS-PpIX, an LED was used as a light source for this study because of its safety toward the cells. Furthermore, they penetrated into the HNSs without loss and reacted with the PpIX located inside the HNSs (Fig. S6, ESI†).[13] The $^1O_2$ generation efficiency of PS is an important factor in PDT. The $^1O_2$ generation was detected by using 9,10-anthracenediyl-bis(methylene)dimalonic acid (ABDA). Fig. S7a (ESI†) presents the decrease of absorbance spectra of ABDA in HNS, PpIX, and FA-HNS-PpIX solutions. The adsorption difference (ΔA) of the FA-HNS-PpIX solution between irradiated and non-irradiated conditions is presented in Fig. 2b. FA-HNS-PpIX exhibited 33.78 % increased $^1O_2$ generation compared to that of equivalent concentration of PpIX (Fig. S7b, ESI†). This result was occurred because of the

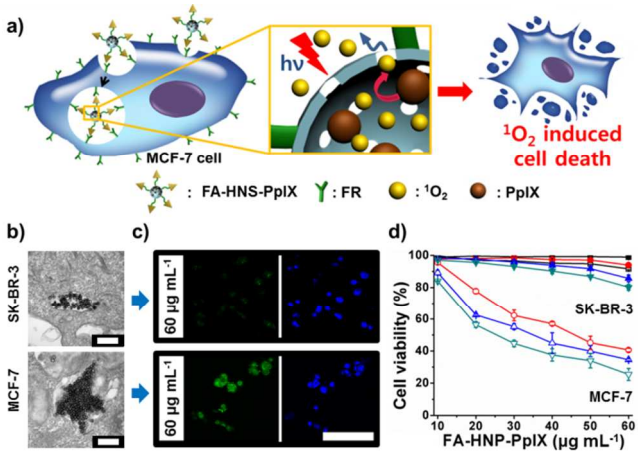

Fig. 3 a) Schematic outline of the PDT of the FA-HNS-PpIX. **b)** TEM images of particle-internalized MCF-7 cells and SK-BR-3 cells were incubated with FA-HNS-PpIX (scale bars: 400 nm). c) Live fluorescence images of FA-HNS-PpIX treated SK-BR-3 and MCF-7 cells (scale bars: 100 μm). Deadend™ fluorescence TdT-mediated dUTP Nick-End Labeling (TUNEL) system stained cell: dead cell (bright green fluorescence), and Fluoroshield™ with 4′,6-Diamidino-2-phenylindole dihydrochloride (DAPI) stained cell: cell nucleus (blue fluorescence). d) Cell viability of MCF-7 (open) and SK-BR-3 (solid) cells with dose and irradiation time dependence (0 min: square, 5 min: circle, 10 min: triangle, and 15 min: inverted triangle symbols). Values exhibit mean ± SD and each experiment was performed in triplicate.

enhanced particle dispersion of FA-HNS-PpIX.[13] By using ABDA, the effective $^1O_2$ generation from FA-HNS-PpIX is assessed under irradiation, which verifies this system is suitable for destructing cancer cell *via* PDT.

The targeting and PDT efficacy of FA-HNS-PpIX were compared using two kinds of human breast cancer cell lines. FR+ MCF-7 cells were used as target cell, while FR- SK-BR-3 cells were control cell. Fig. 3a illustrates the schematic progress of PDT for targeting MCF-7 cells. A specific cell targeting ability is an important factor in PDT system. In order to confirm the targeting ability of FA-HNS-PpIX, the intracellular distribution of HNSs and FA-HNS-PpIX were observed by TEM images (Fig. 3b and S8, ESI†). The FA–HNS–PpIX was more internalized in MCF-7 than SK-BR-3 cells because of the FA-mediated targeting. FA–HNS–PpIX induced PDT was monitored by livecell microscopy to investigate the cancer cell destruction. After the PDT, the dead cells were stained with Deadend™ Fluorometric TUNEL system, which exhibited green fluorescence. Fig. 3c, S11, and S12 (ESI†) shows that the dead cells are more observed in MCF-7 cells while no noticeable cell death is detected in SK-BR-3 cells. To quantify the selective photodynamic efficiency on both cell lines, the viability of the FA–HNS–PpIX-treated cells was determined by cell viability test. Fig. 3d indicates that the cell viability decreases with increasing irradiation time and FA–HNS–PpIX concentration for MCF-7, suggesting that the PDT can be effective under irradiation. For MCF-7 cells, the cell death value is up to 74.5%, which is about *ca.* 3.33 times higher efficiency than in previous reports.[14] Moreover, the PDT activity is more effective on MCF-7 cells than on SK-BR-3 cells because of the active targeting ability of FA. When stored in the dark, the degree of cell death was <10%, meaning that FA–HNS–PpIX has low dark toxicity. The control experiment establishes that HNS, FA–HNS, and HNS–PpIX do not induce significant cell death in both cell lines (Fig. S9, ESI†). This data

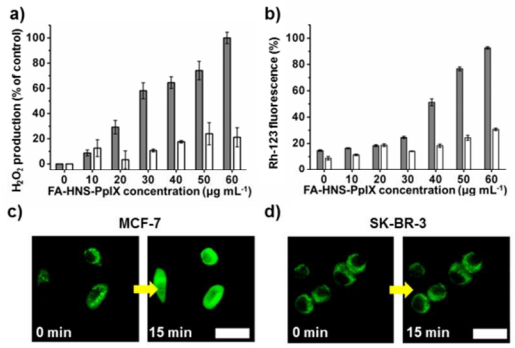

Fig. 4 a) ROS production and b) Rh-123 intensity changes were measured by MCF-7 and SK-BR-3 cells after incubated with different concentration of FA-HNS-PpIX under irradiation (grey: MCF-7, and white: SK-BR-3). Values exhibit mean ± SD and each experiment was performed in triplicate. Live cell fluorescent images of c) MCF-7 cells and d) SK-BR-3 cells. Cells were stained with Rh-123 for visualizing the mitochondrial membrane potential of cells (Scale bars: 30 μm). Mitochondrial dysfunction was observed by MCF-7 cells and SK-BR-3 cells after incubation with 60 μg mL^{-1} of FA-HNS-PpIX and 15min of irradiation.

suggestes that the targeting ability of the FA–HNS–PpIX to FR + MCF-7 cells provides effective tumor destruction under irradiation.

The correlation between the PDT and the cell death was confirmed by monitoring intercellular reactive oxygen species (ROS) generation. The cell damage could be investigated by H_2DCFDA, a intercellular ROS detection dye. Therefore, the FA-HNS-PpIX caused cell damage could be quantified by this ROS generation. In MCF-7 cells, the ROS generation level was increased proportionally with FA-HNS-PpIX concentration and irradiation time (Fig. 4a). In comparison, insignificant ROS production was determined in FR- SK-BR-3 cells. The ROS generation results indicate that FA-HNS-PpIX can lead the cell damages. After investigate the intercellular damage, the mitochondrial function is further detected by monitoring changes in the intensity of Rhodamine-123 (Rh-123) fluorescence, which is a detector of membrane polarization within mitochondria. In general, PDT induced cell damage is mainly caused by the mitochondrial dysfunction. In this regard, the mitochondrial dysfunction can be an indicator of the PDT induced cell death. The mitochondrial function was investigated by Time-lapsed livecell fluorescence imaging. The significant fluorescence change in MCF-7 cells showed the mitochondrial membrane potential depolarization. The Rh-123 intensity increased proportionally with irradiation time and FA–HNS–PpIX concentration in MCF-7 cells (Fig. 4b, c and d). In SK-BR-3 cells, there is no obvious difference between negative and FA–HNS–PpIX-treated cells, meaning that SK-BR-3 is remained as healthy cells. Judging from these data, the $^1O_2$ caused this mitochondrial membrane potential depolarization and eventually led cell death.[15] Collectively, under irradiation, PDT induced mitochondrial damage, and cell death. Our FA-HNS-PpIX system has specific cell targeting ability for FR + MCF-7 cells. Moreover, this system efficiently destructed MCF-7 cells and suitable for PDT without any harm to FR- normal cells.

In summary, monodisperse HNSs were loaded with photosensitizer PpIX, and the surface was functionalized with FA. LED light was used as a PDT light source to minimize photodamage to normal cells. We systematically investigated the effect of FA–HNS–PpIX on the cells for investigating PDT efficacy, particle uptake, and cell damage. Under the same experimental conditions, low cell death was shown in SK-BR-3 cells, while high cell death was observed in MCF-7 cells because of active targeting of FA. FA–HNS–PpIX was *ca.* 3.33 times more efficient than previous examples for the same cell death level. Moreover, FA–HNS–PpIX exhibited low dark toxicity, efficient PpIX delivery with selectivity. Therefore, the FA–HNS–PpIX system offers a practical new direction for PDT.

Notes and references

1. (a) M. Wu, W. Gunning and M. Ratnam, *Cancer Epidemiol., Biomarkers Prev.*, 1999, **8**, 775; (b) J. Nordberg and E. S. J. Arnér, *Free Radicals Biol. Med.*, 2001, **31**, 1287.
2. Y. Zhang, J. Qian, D. Wang, Y. Wang and S. He, *Angew. Chem., Int. Ed.*, 2013, **52**, 1148.
3. (a) D. Bartczak, O. L. Muskens, T. M. Millar, T. Sanchez Elsner and A. G. Kanaras, *Nano Lett.*, 2011, **11**, 1358; (b) D. O. Lapotko and V. P. Zharov, *Lasers Surg. Med.*, 2005, **36**, 22.
4. Y. Yang, Q. Guo, H. Chen, Z. Zhou and Z. Shen, *Chem. Commun.*, 2013, **49**, 3940.
5. W. K. Oh, S. Kim, M. Choi, C. Kim, Y. S. Jeong, B. R. Cho, J. S. Hahn and J. Jang, *ACS nano*, 2010, **4**, 5301.
6. (a) C. Kim, S. Kim, W. K. Oh, M. Choi and J. Jang, *Chem. Eur. J.*, 2012, **18**, 4902; (b) Z. H. Chen, C. Kim, X. b. Zeng, S. H. Hwang, J. Jang and G. Ungar, *Langmuir*, 2012, **28**, 15350.
7. (a) K. Li, Y. Jiang, D. Ding, X. Zhang, Y. Liu, J. Hua, S. S. Feng and B. Liu, *Chem. Commun.*, 2011, **47**, 7323; (b) L. Yan, W. Chen, X. Zhu, L. Huang, Z. Wang, G. Zhu, V. A. L. Roy, K. N. Yu and X. Chen, *Chem. Commun.*, 2013, **49**, 10938.
8. M. Choi, C. Kim, S. O. Jeon, K. S. Yook, J. Y. Lee and J. Jang, *Chem. Commun.*, 2011, **47**, 7092.
9. G. Bogush, M. Tracy and C. Zukoski, *J. Non-Cryst. Solids*, 1988, **104**, 95.
10. A. R. Loiola, J. C. R. A. Andrade, J. M. Sasaki and L. R. D. da Silva, *J. Colloid Interface Sci.*, 2012, **367**, 34.
11. (a) G. Socrates and G. Socrates, *Infrared and Raman characteristic group frequencies: tables and charts*, 3rd edn., Wiley, Chichester ; New York, 2001, 347; (b) J. Avalani, D. Patel and D. Raval, *J. Chem. Sci.*, 2012, **124**, 1091.
12. J. X. Chen, H.-Y. Wang, C. Li, K. Han, X.-Z. Zhang, R.-X. Zhuo, *Biomaterials* 2011, **32**, 1678.
13. R. A. Hsi, D. I. Rosenthal and E. Glatstein, *Drugs*, 1999, **57**, 725.
14. X. Liang, X. Li, X. Yue and Z. Dai, *Angew. Chem., Int. Ed.*, 2011, **50**, 11622.
15. J. J. Lemasters, A. L. Nieminen, T. Qian, L. C. Trost, S. P. Elmore, Y. Nishimura, R. A. Crowe, W. E. Cascio, C. A. Bradham and D. A. Brenner, *Biochim. Biophys. Acta, Bioenerg.*, 1998, **1366**, 177.